crystals

MDPI

Article

Static Recrystallization Microstructure Evolution in a Cold-Deformed Ni-Based Superalloy during Electropulsing Treatment

Hongbin Zhang, Chengcai Zhang, Baokun Han, Kuidong Gao, Ruirui Fang, Nana Deng and Haiping Zhou *

College of Mechanical and Electronic Engineering, Shandong University of Science and Technology, Qingdao 266590, China; zhanghb@sdust.edu.cn (H.Z.); skd996028@sdust.edu.cn (C.Z.); skd990444@sdust.edu.cn (B.H.); gaokuidong@sdust.edu.cn (K.G.); fangruirui123@gmail.com (R.F.); dengnana123@gmail.com (N.D.)

* Correspondence: zhouhp@sdust.edu.cn

Received: 12 August 2020; Accepted: 28 September 2020; Published: 30 September 2020

Abstract: The influence of electropulsing treatment (EPT) parameters on the static recrystallization (SRX) microstructure in a cold-deformed Ni-based superalloy was investigated. During EPT, both the volume fraction of SRX grains and the average grain size increased with the increasing EPT temperature, which was attributed to the thermal effect and athermal effect induced by EPT. The mobility of SRX grain boundaries was promoted at the higher temperature due to the thermal effect, while the nucleation rate would be increased by EPT through decreasing the thermodynamic barrier. The formation of parallel dislocations caused by electron wind force could also play an indirect role in promoting SRX process. Moreover, the volume fraction of SRX grains increased significantly with the extension of EPT time at 700 °C, while the EPT time had a trivial effect on the average grain size. In addition, the sufficient deformation was essential to the occurrence of SRX behavior during EPT, and the localized Joule heating effect could promote the SRX behavior in the samples with the larger strains. Besides that, the influence of twining and carbides on the SRX behaviors was also investigated.

Keywords: electropulsing treatment; static recrystallization; Ni-based superalloy; cold-rolling deformation

1. Introduction

Ni-based superalloys have been widely applied in the aerospace field, because of their extraordinary mechanical properties and corrosion resistance under the critical and severe service conditions [1–3]. With the rapid development of aerospace industry, the working conditions of Ni-based superalloys have become more and more severe, and the higher requirements for alloy properties are also put forward [4]. Due to the fact that Ni-based superalloys belong to crystalline materials, optimization of crystal structures is considered to be one of the most effective methods for strengthening Ni-based superalloys [5]. In this case, grain refinement via recrystallization has become a commonly employed approach, and the equiaxed fine crystal structures induced by recrystallization can significantly contribute to the mechanical properties of Ni-based superalloy parts, such as turbine discs [3]. Meanwhile, the desired crystalline structures could be achieved through the proper process of deformation and heat treatment. The free energy of crystalline material would be raised during deformation by the presence of defects, which could be effectively removed or alternatively arranged in configurations of lower energy via recrystallization during the subsequent heating process [6]. Thus, further research on the recrystallization microstructure evolution of Ni-based superalloys during the deformation and heat treatment process is very important for improving their mechanical properties.

Heat treatment is a vital process to control the recrystallization microstructure in the deformed alloys [7]. However, the conventional heat treatment (CHT) usually required a long time to achieve the equilibrium states or para-equilibrium states before the cooling process, which are not only low heating efficiency, but high energy consumption [8]. In the past few decades, fast heat treatment processes, such as the electropulsing treatment (EPT), have attracted more and more attention, which can cause the dramatic changes on the microstructure and mechanical behavior of alloys [9–11]. As an effective fast-heating approach, EPT can effectively optimize the crystal structures, such as the grain refinement in solid state through accelerating the kinetic of recrystallization [12,13].

The positive effect of EPT on the recrystallization behavior of different alloys had been revealed by many studies. For example, Ao et al. [12] found that EPT effectively promoted the recrystallization behavior of Ti-6Al-4V alloy with extremely short-time under a relative low temperature, comparing to the traditional heat treatment. Yu et al. [13] investigated the effect of EPT on grain refinement of a medium carbon low alloy steel, and it was found that EPT could decrease the potential barriers for recrystallization nucleation and increase its rate. Guo et al. [14] studied the influence of EPT on the recrystallization behavior of cold-rolled Mg alloy ZK60 strips, and it was found that the nucleation rate and migration ability of grain boundaries were significantly promoted by EPT, leading to the acceleration of recrystallization behavior at the relatively low temperature. In the authors' previous publication [8], it was reported that the SRX behaviors were significantly accelerated by EPT in a typical cold-deformed Ni-based superalloy. At present, there were only a few studies about the influence of EPT on the Ni-based superalloy, while the research on the static recrystallization (SRX) microstructure evolution during EPT was very limited.

In this work, the EPT combined with cold-rolling process was used to optimize the SRX microstructure of a Ni-based superalloy. Meanwhile, the dependence of SRX microstructure on the processing parameters was investigated, and the parameters were optimized. In addition, the underlying mechanisms were also discussed in detail.

2. Experimental Procedures

The Ni-based superalloy in this investigation was GH3030 alloy, which was provided by Fushun special steel Co. Ltd (Fushun, China). At present, GH3030 alloy has attracted growing interest in the aerospace field, owing to the excellent oxidation resistance, high thermal strength, and good plasticity [15]. The nominal chemical composition of GH3030 alloy is listed in Table 1.

Table 1. Nominal chemical composition of GH3030 alloy (wt. %).

Element	C	Cr	Ni	Ti	Al
wt. %	≤0.12	19.0–22.0	Bal.	0.15–0.35	≤0.15
Element	Fe	Mn	Si	P	S
wt. %	≤1.5	≤0.7	≤0.8	≤0.03	≤0.02

Prior to EPT, the pretreatment of GH3030 alloy was carried out, including solution treatment (1130 °C, 2 h) and cold-rolling deformation with the strains of 0.3, 0.5, and 0.7. The microstructure of GH3030 alloy after solution treatment was reported in the authors' previous publication [16], which is shown in Figure 1. Figure 1a shows the inverse pole figure (IPF) of the initial microstructure after solution treatment, in which the high angle grain boundaries (HAGBs) were represented by the black lines. It can be seen that the grain size was relatively uniform, the distribution of which is shown in Figure 1b. The average grain size of GH3030 alloy after solution treatment was 11.2 ± 2.6 μm.

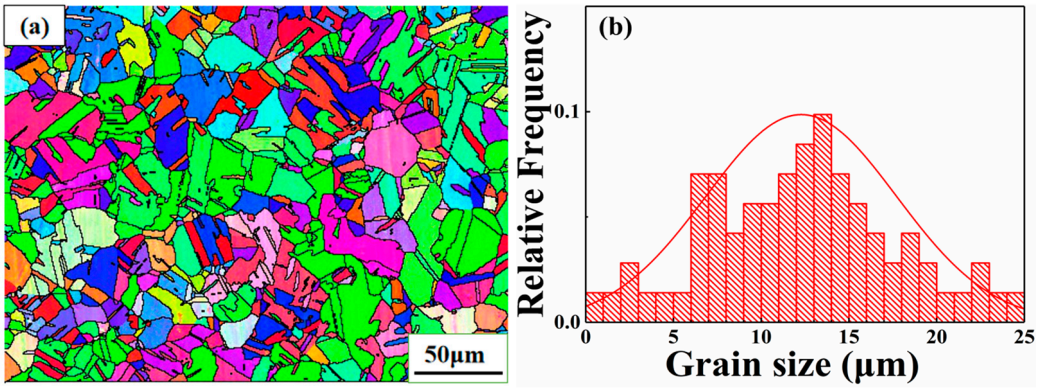

Figure 1. (**a**) Inverse pole figure (IPF) map of GH3030 alloy after solution treatment [16], (**b**) grain size distribution of GH3030 alloy after solution treatment.

After solution and cold-rolling, the samples were machined into strips along the rolling direction, with the cross-section of 5 mm × 1 mm, and underwent surface polishing. Then, the EPT process of these strips was carried out by utilizing a self-made apparatus, which was introduced in the previous publication [16]. The EPT parameters were chosen at 700–900 °C for 10–30 min, and the K-type thermocouple was utilized for temperature measurements. After EPT, the strips were rapidly quenched in the water to room temperature.

The SRX microstructure of EPT samples was measured by using both the electron backscattered diffraction (EBSD) and transmission electron microscope (TEM) technique. The EBSD characterization was executed on a TESCAN MAIA3 scanning electron microscope, and the measured data were analyzed by HKL-Channel 5 software. In order to ensure the high quality of EBSD images, the zero solution of each EBSD image was less than 4%, and the mean angular deviation (MAD) was less than 0.5°. Meanwhile, the EBSD scan step was set to 0.6~1 μm, and the clean-up procedure would be executed prior to data analysis. In addition, the internal average misorientation within the grain was measured to evaluate the fraction of recrystallized, substructured, and deformed grains. According to the average misorientation θ', the grains were classified into recrystallized ($\theta' \leq 2°$), substructured ($2° < \theta' < 7.5°$), and deformed ($\theta' \geq 7.5°$) grains. Moreover, a JEM-200 EX microscope was employed for TEM observation, in order to further analyze the SRX microstructure, dislocations, carbides, twins, and so on. The thin foils for TEM observation were cut from the EPT strips, and then mechanically thinned to 100 μm. After that, the thin foils were further twin-jet electro-polished by utilizing a mixed acid solution of 10% perchloric acid and 90% ethanol.

3. Results and Discussion

3.1. Effect of EPT Temperature on the SRX Microstructure

Figure 2 shows the EBSD orientation mapping with grain size distribution of EPT samples treated at different temperatures for 20 min, where the rolling direction (RD) was indicated. The SRX grains, sub-grains, and deformed grains were distinguished, which were represented by blue, yellow, and red colors, respectively. From Figure 2, it can be found that the EPT temperature had a great influence on the microstructures of the cold-deformed Ni-based superalloy. As shown in Figure 2a, a lot of fine SRX grains were formed at 700 °C, and some sub-grains can also be observed. Meanwhile, very few deformed grains remained, indicating the good development of SRX behaviors. With the increasing EPT temperature, the coarsening of SRX grains was very obvious, as shown in Figure 2c–e, which could be realized via absorbing defective neighboring grains. Meanwhile, the volume fractions of sub-grains and deformed grains decreased gradually with the increasing EPT temperature, which were replaced by the SRX grains. The increasing energy provided by EPT became the driving force for the good development of SRX behaviors.

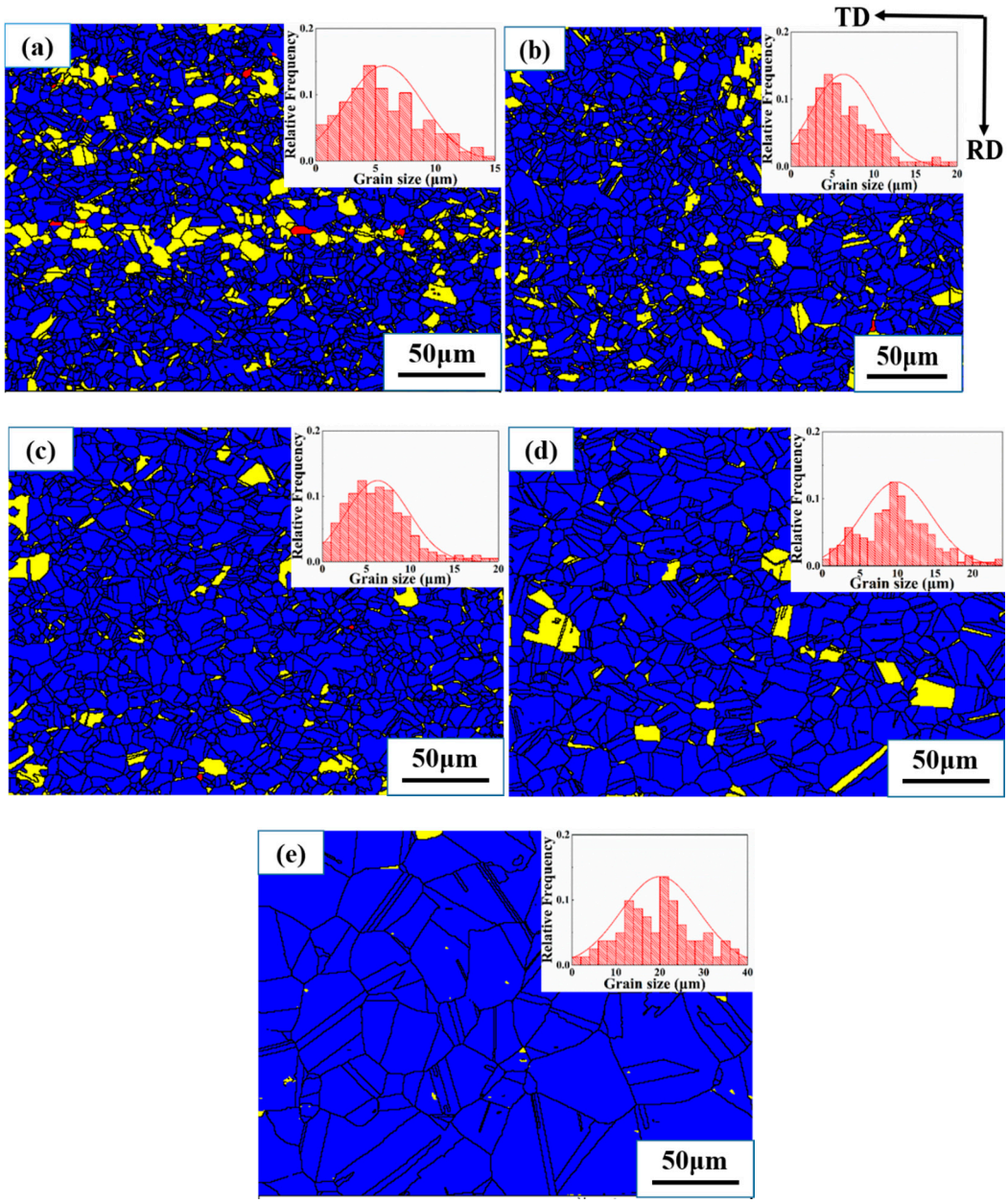

Figure 2. Electron backscattered diffraction (EBSD) orientation mapping with grain size distribution of electropulsing treatment (EPT) samples treated at different temperatures for 20 min: (**a**) 700 °C, (**b**) 750 °C, (**c**) 800 °C, (**d**) 850 °C, and (**e**) 900 °C.

From Figure 2, it also can be seen that the EPT temperature had a significant influence on the grain size distribution. The distribution range of grain size became wider and wider with the increasing EPT temperature. Comparing with the initial microstructure after solution treatment, the distribution range of grain size was obviously narrower in the EPT samples treated below 800 °C. Additionally, the peak value of grain size distribution moved towards the right with the increasing EPT temperature, indicating the occurrence of grain growth.

The above phenomena were considered to be closely related to the thermal effect (Joule heating effect) and athermal effect during EPT. It has been reported that both the thermal effect and athermal effect would affect the recrystallization process, the free energy change of which (ΔW) can be written as [17–19]:

$$\Delta W = \Delta W_0 + \Delta W_e \quad (1)$$

$$\Delta W_e = K\zeta(\sigma_2, \sigma_1)\Delta V j^2 \quad (2)$$

where ΔW_0 is the free energy change in the system without EPT, and ΔW_e is the free energy change owing to the introduction of pulsed current. In Equation (2), K is a positive constant, while ΔV and j are the volume of a nucleus and current density, respectively. Moreover, $\zeta(\sigma_2, \sigma_1)$ can be expressed by the following formula [18]:

$$\zeta(\sigma_2, \sigma_1) = (\sigma_1 - \sigma_2)/(\sigma_2 + 2\sigma_1) \quad (3)$$

where σ_1 and σ_2 are the conductivity of deformed and recrystallization microstructure. Comparing to the recrystallization microstructure, there are more crystal defects, such as dislocations, in the deformed microstructure, resulting in that $\sigma_1 < \sigma_2$. Then, combining Equations (2) and (3), it can be concluded that $\Delta W_e < 0$. On the basis of the classical nucleation theory, the average number of stable nuclei (n) can be calculated by [19]:

$$n = n_0 \cdot \exp(-\frac{W_C}{kT}) \quad (4)$$

$$W_C = \max\{\Delta W\} \quad (5)$$

where n_0 is the total number of atoms in the system, k is Boltzmann's constant, and T is temperature. Obviously, the higher temperature could promote the nucleation of the recrystallization process. Meanwhile, it should be noted that W_C is the thermodynamic barrier of the formation of a spherical nucleus with critical radius, which is closely related to ΔW. Due to the fact that $\Delta W_e < 0$, it is obvious that ΔW in a current-carrying system is lower than that in the system without EPT. In other words, there are more stable nuclei in the current-carrying system, while the nucleation rate can be increased by EPT through decreasing the thermodynamic barrier.

Figure 3 shows the volume fractions of different kinds of grains and the average grain size of EPT samples treated at different temperatures for 20 min. As shown in Figure 3a–c, it can be found that the volume fraction of SRX grains reached above 80% for the samples treated at different EPT temperatures, which was much larger than those of sub-grains and deformed grains. Meanwhile, the volume fraction of SRX grains increased with the increasing EPT temperature, which reached around 99% at 900 °C. During EPT process, the directional flow of electrons could promote the movement of dislocations, as a result of the electromigration effect [9], which is beneficial to the development of SRX behavior. Meanwhile, the electromigration effect could play a more significant role in promoting the SRX behaviors at the higher current density, i.e., the higher EPT temperature. Comparing with SRX grains, the volume fractions of sub-grains and deformed grains exhibited the opposite trend, which decreased with the increasing EPT temperature. Their fractions were even less than 1% at 900 °C, indicating that almost all the sub-grains and deformed grains had been replaced by SRX grains. Besides the athermal effect during EPT, the mobility of SRX grain boundaries would also be promoted at the higher temperature owing to the thermal effect [20]. On the other hand, the average grain size increased with the increasing EPT temperature, as shown in Figure 3d. The average grain size was less than 6.5 μm in the samples treated at 700 °C. Meanwhile, the grain size distribution was very uniform at 700 °C, as shown in Figure 2a. In other words, the grain refinement was realized at the low EPT temperature, which is beneficial to the mechanical properties of Ni-based superalloy. As mentioned above, the SRX behavior could be promoted by the thermal and athermal effect during EPT. The athermal effect could accelerate SRX nucleation rate, and the thermal effect could significantly contribute to the growth of SRX grains. Thus, the low EPT temperature was conducive to realizing the refinement of SRX grains during EPT, due to the weakened thermal effect.

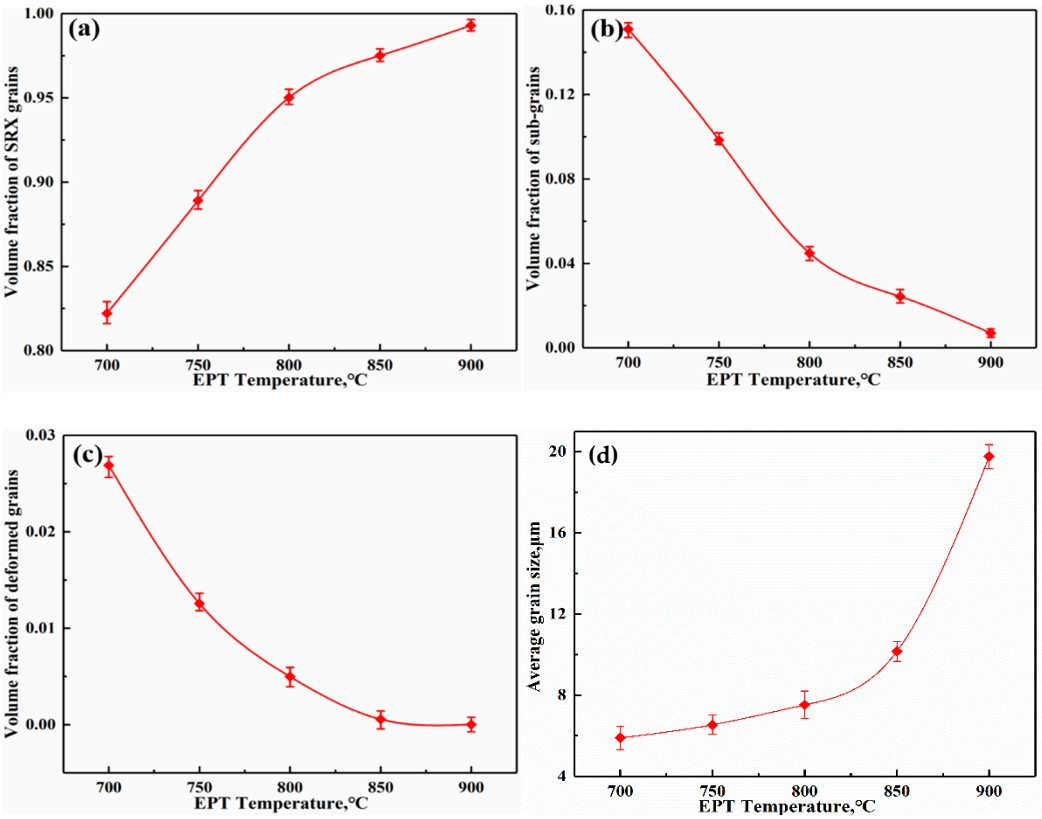

Figure 3. Volume fractions of SRX grains (**a**), sub-grains (**b**), deformed grains (**c**), and average grain size (**d**) of EPT samples treated at different temperatures for 20 min.

In order to further study the microstructure evolution of the cold-deformed Ni-based superalloy during EPT, TEM observations were also carried out. Figure 4 shows the TEM images of EPT samples treated at different temperatures. As shown in Figure 4a, some new SRX nuclei can be clearly seen, in which there was almost no dislocations. The formation of SRX nuclei could be promoted by EPT via reducing potential barriers for nucleation and increasing nucleation rate [21]. At 800 °C, the triple-junction grain boundary can be clearly observed in Figure 4c. Meanwhile, there were some dislocations around the straight grain boundaries, which would be absorbed by the boundaries of SRX grains. Interestingly, the parallel dislocations can be clearly observed in the samples treated at different temperatures, as shown in Figure 4b,d, which were mainly caused by electron wind force during EPT. It is well known that the electron wind force could make the dislocations mobile [8,22]. As a result, the dislocations would be aligned along the current direction, leading to the formation of parallel dislocations. Under the effect of electron wind force, the dislocations would also be accumulated around the boundaries of sub-grains, while annihilated on the boundaries with small angle misorientation via climbing, resulting in the formation of more misoriented sub-grains [22]. Meanwhile, these sub-grains with larger misoriented boundaries were suitable for SRX nucleation.

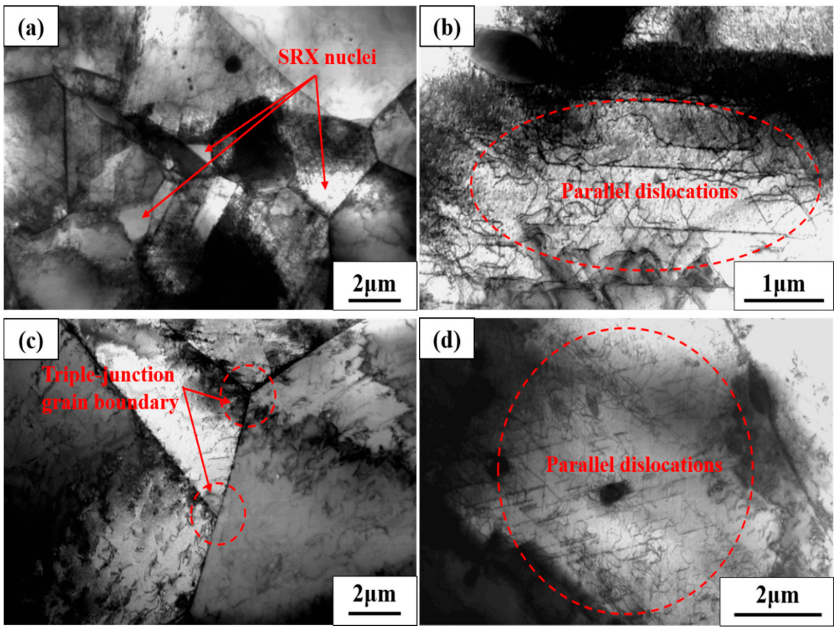

Figure 4. Transmission electron microscope (TEM) images of EPT samples treated at different temperatures for 20 min: (**a**,**b**) 700 °C and (**c**,**d**) 800 °C.

3.2. Effect of EPT Time on the SRX Microstructure

According to the fine grain structure of the samples treated at 700 °C, the EBSD orientation mapping of EPT samples treated at 700 °C for different lengths of time were also analyzed, as shown in Figure 5. As shown in Figure 5a, there were many sub-grains in the structures, but few deformed grains can be observed. The nucleation of SRX grains was closely related to the coalescence of sub-grains [3]. Meanwhile, the deformed grains were easy to recrystallize during EPT, and the deformation stored energy would be released during the recrystallization process [23]. As shown in Figure 5b,c, it can be found that the sub-grains and deformed grains were gradually replaced by the SRX grains with EPT proceeding, whilst the grain size had no remarkable change. There was little change in grain size distribution, both the range and the peak value of which varied little. The similar phenomenon was also reported in the cold-rolled magnesium alloy ZK60 during EPT [14]. In the EPT samples treated for 30 min, the recrystallization process was almost completed, and almost no deformed grains could be seen, as shown in Figure 5c.

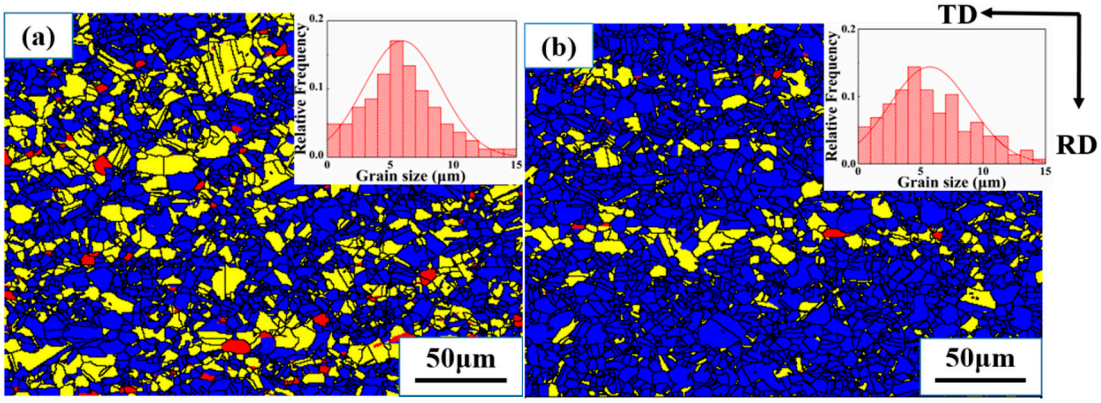

Figure 5. *Cont.*

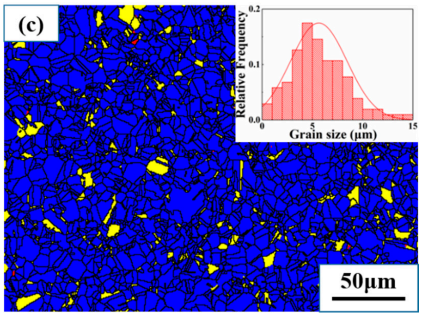

Figure 5. EBSD orientation mapping with grain size distribution of EPT samples treated at 700 °C for different lengths of time: (**a**) 10 min, (**b**) 20 min, and (**c**) 30 min.

Figure 6 shows the volume fractions of different kinds of grains and average grain size of EPT samples treated at 700 °C for different lengths of time. It can be found that both the volume fraction of SRX grains and the average grain size increased with the increasing EPT time, as shown in Figure 6a,d. In contrast, the volume fractions of sub-grains and deformed grains decreased with the increasing EPT time, as shown in Figure 6b,c. For the EPT samples treated for 10 min, the volume fraction of SRX grains was below 60%, which significantly increased above 90% after treating for 30 min. Comparing to the volume fraction of SRX grains, the EPT time had a trivial effect on the average grain size, which increased no more than 0.6 μm after treating for 30 min. When the EPT time was prolonged, the sub-grains were gradually transformed into SRX grains, and there was more time for the development of the recrystallization process, resulting in the increasing volume fraction of SRX grains. In other words, the increasing EPT time provided the suitable circumstances for the development of SRX behaviors, which could facilitate annihilation of dislocations. From the point of energy, there would be more input energy from pulsed current with the increasing EPT time, which provided more energy for the nucleation of SRX grains. Moreover, the low temperatures restricted the grain growth, resulting from the low thermal effect. In a word, although the low EPT temperature was conducive to obtaining fine SRX grains, enough EPT time was also necessary to increase the volume fraction of SRX grains.

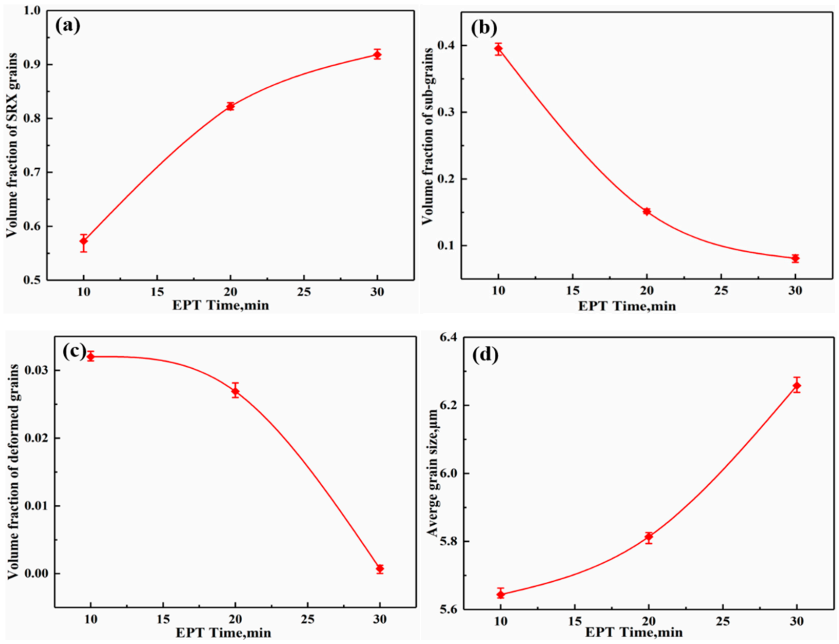

Figure 6. Volume fractions of SRX grains (**a**), sub-grains (**b**), deformed grains (**c**), and average grain size (**d**) of EPT samples treated at 700 °C for different lengths of time.

3.3. *Effect of Deformation Strain on the SRX Microstructure*

It is well known that the stored energy induced by deformation can be released through recrystallization [23], and thus deformation strain should also be an important factor affecting the SRX behavior during EPT. Figure 7 shows the EBSD orientation mapping with grain size distribution of EPT samples treated at 700 °C for 30 min with different strains. As shown in Figure 7a, the structure mainly consisted of deformed grains and sub-grains, while very few SRX grains can be observed along the grain boundaries, which was a typical feature of partial recrystallization. Such phenomenon indicated that the low strain of 0.3 did not provide enough deformation energy for the development of the recrystallization process. As shown in Figure 7b,c, it can be found that the large strains significantly promoted the occurrence of the recrystallization process, and more SRX grains can be observed in the samples with the larger deformation strains.

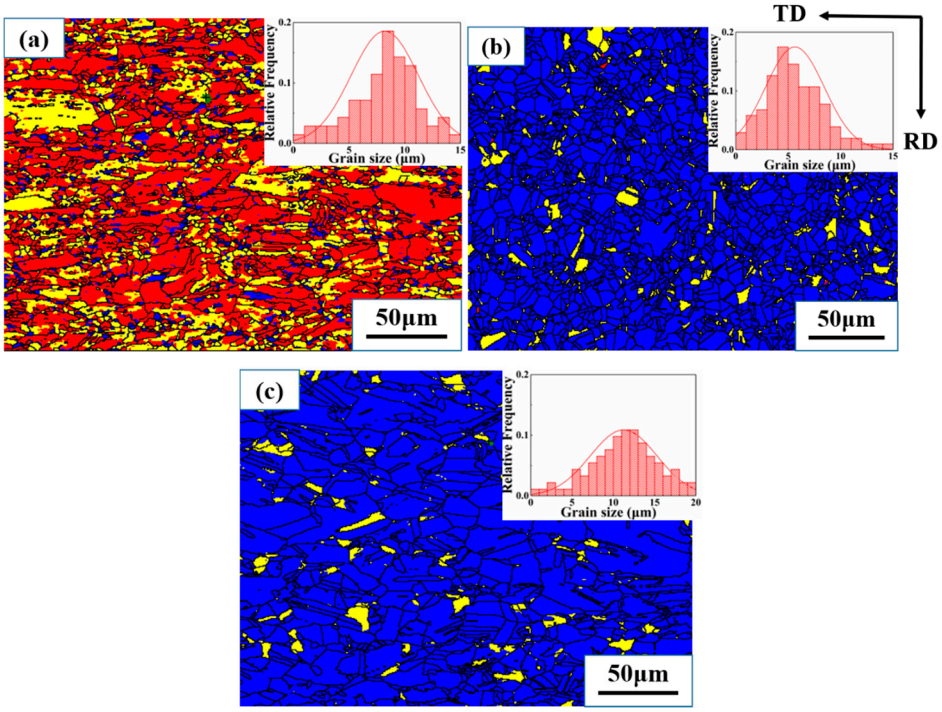

Figure 7. EBSD orientation mapping with grain size distribution of EPT samples treated at 700 °C for 30 min with different strains: (**a**) 0.3, (**b**) 0.5, and (**c**) 0.7.

Besides having sufficient deformation stored energy and nucleation sites, there might be other reasons for the good development of SRX process in the samples with the larger strains during EPT. The dislocation density was higher in the samples with larger strains, which had a higher electrical resistivity. Owing to the Joule heating effect during EPT, the higher resistivity would produce a local higher temperature field around the dislocations [24,25]. Such phenomenon would cause the formation of micro-scaled inhomogeneous temperature fields, although the measured macro-scaled temperature field in the alloy was still uniform. The localized Joule heating effect could promote the SRX behavior in the samples with the larger strains during EPT. Besides that, it has been reported that the athermal effect was considered to be higher in the samples with the larger strains [14], which can also promote the nucleation of SRX grains. On the other hand, the peak value of grain size distribution moved towards the left firstly, and then towards the right with the increasing strains. The former was related to the good development of SRX behaviors, and the latter was attributed to the growth of SRX grains at the large strain of 0.7.

Figure 8 shows the volume fractions of different kinds of grains and average grain size of EPT samples treated at 700 °C for 30 min with different strains. In the samples with the low strain of

0.3, the volume fraction of SRX grains was only 10%, as shown in Figure 8a. When the deformation strains increased above 0.5, the volume fraction of SRX grains reached above 90%, indicating that the sufficient deformation was essential to the occurrence of SRX behavior during EPT. Obviously, the nucleation rate would be increased markedly with the increasing strains, mainly owing to the higher deformation stored energy, the larger area of potential nucleation sites, and localized Joule heating effect. As shown in Figure 8b,c, it can be seen that the volume fractions of sub-grains and deformed grains decreased with the increasing strains, while the decreasing rate of deformed grains was much larger. At the strains above 0.5, the volume fraction of deformed grains was even no more than 0.5%. In addition, the average grain size decreased firstly and then increased with the increasing deformation strains, which exhibited a minimum value of 6.75 μm in the samples with strain of 0.5, as shown in Figure 8d. At the low strain of 0.3, the full recrystallization was not completed, and there were many large deformed grains in the structures, as mentioned above. For the samples with the large strain of 0.7, the high stored energy could significantly promote the grain boundary migration, leading to the growth of SRX grains.

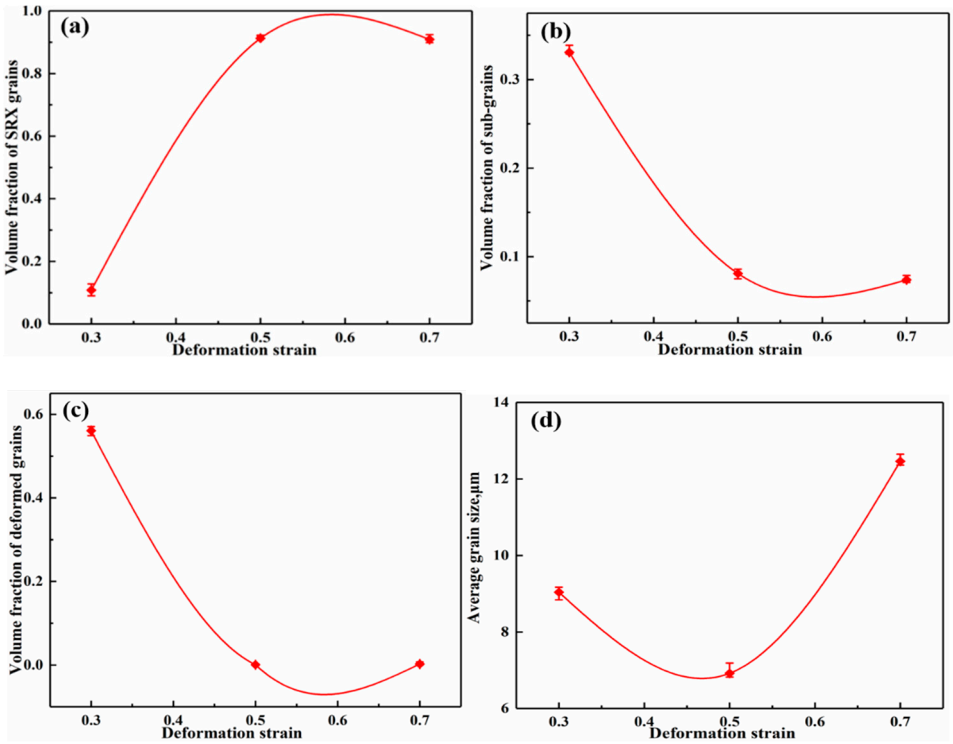

Figure 8. Volume fractions of SRX grains (**a**), sub-grains (**b**), deformed grains (**c**), and average grain size (**d**) of EPT samples treated at 700 °C for 30 min with different strains.

Figure 9 shows the TEM images of EPT samples treated at 700 °C for 30 min with the strain of 0.5, and the selected area diffraction (SAD) patterns. As shown in Figure 9a, the annealing twins can be clearly seen, which were newly formed in the SRX grains. Figure 9b shows the SAD pattern of the annealing twins. The high mobility migration of SRX grain boundaries during EPT could promote the formation of stacking errors at some locations of high angle grain boundaries, and thus promoting the nucleation of annealing twins [16]. Meanwhile, twining can play an important role in the development of recrystallization process [26–28]. It has been reported that twining would contribute to the nucleation of SRX grains via promoting separation of bulged parts from original grains [26]. In addition, twinning would reorient grain boundaries to stimulate the dislocation absorption and mobility of grain boundaries during the recrystallization process, and thus it could resume the growth of SRX grains, once which became stagnant [27,28].

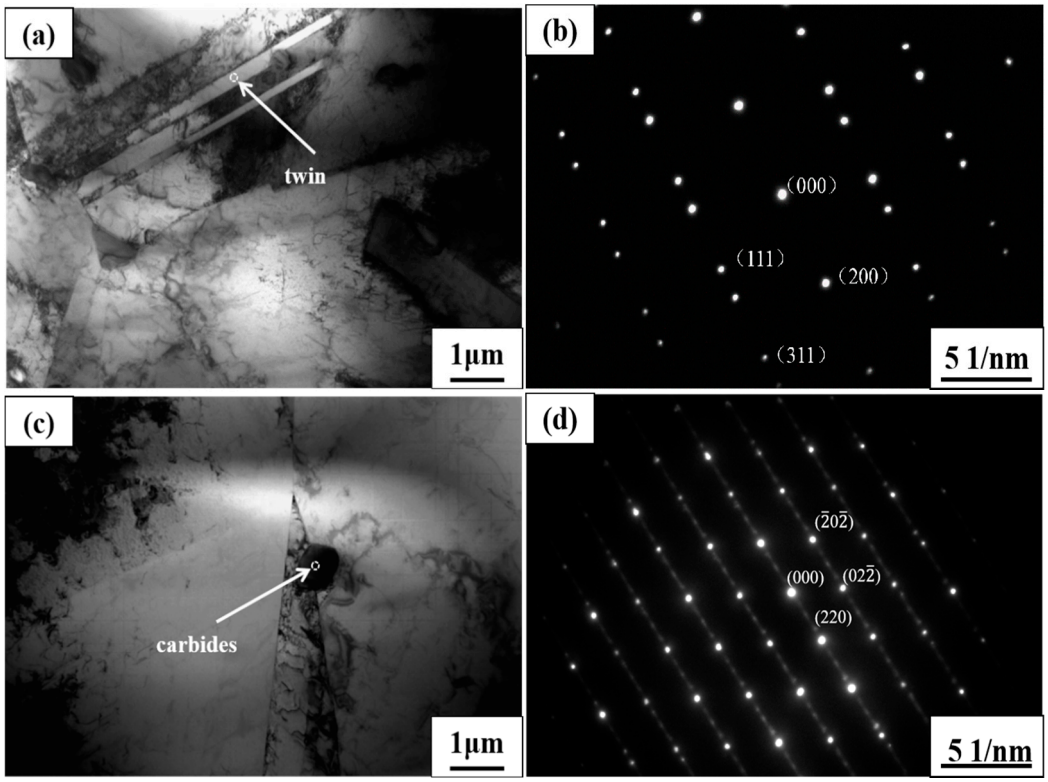

Figure 9. TEM images of EPT samples treated at 700 °C for 30 min with the strain of 0.5 (**a**,**c**), and the corresponding selected area diffraction (SAD) patterns of annealing twins (**b**) and carbide (**d**).

As shown in Figure 9c, a typical carbide can be clearly seen around the grain boundaries, and its SAD pattern was given in Figure 9d. Due to the acceleration of atom diffusion and more vacancies produced by EPT [29], the precipitation of carbides will be promoted, and their growth rate will also increase. During EPT, the migration of grain boundaries and dislocations would be hindered by these carbides, and thus the pinning effect of carbides could inhibit the growth of SRX grains. In other words, EPT had a positive effect on the precipitation and growth of carbides, which played an indirect role in grain refinement.

4. Conclusions

In this study, the SRX microstructure evolution in a cold-deformed Ni-based superalloy during EPT was studied, and the underlying mechanisms were also discussed in detail. It was found that both the volume fraction of SRX grains and the average grain size increased with the increasing EPT temperature, and the volume fraction of SRX grains reached around 99% after treating for 20 min at 900 °C. The mobility of SRX grain boundaries was promoted at the higher temperature owing to the thermal effect, and the nucleation rate could be increased by EPT through decreasing the thermodynamic barrier. Meanwhile, the grain refinement was realized via SRX process at the low EPT temperature, and the average grain size was less than 6.5 μm in the samples treated at 700 °C for 20 min. In addition, due to the effect of electron wind force during EPT, the parallel dislocations were formed in the samples treated at different temperatures, which could play an indirect role in promoting the SRX process.

With the increasing EPT time, there was more time for the development of the recrystallization process, leading to the increasing volume fraction of SRX grains. For the EPT samples treated at 700 °C for 10 min, the volume fraction of SRX grains was below 60%, which increased above 90% after treating for 30 min. By comparison, the EPT time had a trivial effect on the average grain size at 700 °C, which increased no more than 0.6 μm after treating for 30 min. Besides EPT temperature

and time, the sufficient deformation was also essential to the occurrence of SRX behavior during EPT, and the localized Joule heating effect could promote the SRX behavior in the samples with larger strains. Meanwhile, the average grain size decreased firstly and then increased with the increasing deformation strains at 700 °C, which exhibited a minimum value in the samples with the strain of 0.5.

Author Contributions: Investigation, H.Z. (Hongbin Zhang), C.Z., B.H., K.G., R.F., N.D., H.Z. (Haiping Zhou); resources, B.H., K.G.; writing—original draft preparation, H.Z. (Hongbin Zhang), C.Z.; writing—review and editing, H.Z. (Hongbin Zhang), H.Z. (Haiping Zhou); project administration, H.Z. (Hongbin Zhang); funding acquisition, H.Z. (Hongbin Zhang), H.Z. (Haiping Zhou), K.G. All authors have read and agreed to the published version of the manuscript.

Funding: This work has been supported by the National Natural Science Foundation of China (No. 51804187 and 51904176), Project funded by China Postdoctoral Science Foundation (No. 2019M662400), Project of Shandong Province Higher Educational Young Innovative Talent Introduction and Cultivation Team (Performance enhancement of deep coal mining equipment), and Qingdao post-doctoral researcher applied research programs.

Conflicts of Interest: The authors declare no conflict of interest.

References

1. Zhang, H.; Zhang, K.; Jiang, S.-S.; Zhou, H.; Zhao, C.; Yang, X. Dynamic recrystallization behavior of a γ′-hardened nickel-based superalloy during hot deformation. *J. Alloy Compd.* **2015**, *623*, 374–385. [CrossRef]
2. Ji, R.; Zheng, Q.; Liu, Y.; To, S.; Yip, W.S.; Yang, Z.; Jin, H.; Wang, H.; Cai, B.; Cheng, W. An investigation of mechanical-thermal coupling treatment on material properties, surface roughness, and cutting force of Inconel 718. *Int. J. Adv. Manuf. Technol.* **2019**, *105*, 1917–1931. [CrossRef]
3. Wang, R.; Xu, Q.; Gong, X.; Su, X.; Liu, B. Experimental and numerical studies on recrystallization behavior of single-crystal Ni-base superalloy. *Materials* **2018**, *11*, 1242. [CrossRef]
4. Liu, Y.; Wang, L.; Liu, H.-Y.; Zhang, B.-J.; Zhao, G.-P. Effect of electropulsing treatment on corrosion behavior of nickel base corrosion-resistant alloy. *Trans. Nonferrous Met. Soc. China* **2011**, *21*, 1970–1975. [CrossRef]
5. Zhang, H.; Zhang, K.; Zhou, H.; Lu, Z.; Zhao, C.; Yang, X. Effect of strain rate on microstructure evolution of a nickel-based superalloy during hot deformation. *Mater. Des.* **2015**, *80*, 51–62. [CrossRef]
6. Humphreys, F.; Hatherly, M. *Recrystallization and Related Annealing Phenomena*; Pergramon Press: London, UK, 2004.
7. Zhang, J.; Hu, P.; Li, X. Effect of starting microstructure in high speed steel on the grain refinement potency of electropulsing treatment. *IOP Conf. Series: Mater. Sci. Eng.* **2020**, *711*, 012009. [CrossRef]
8. Han, K.; Qin, S.; Li, H.; Liu, J.; Wang, Y.; Zhang, C.; Zhang, P.; Zhang, S.; Zhang, H.; Zhou, H. EBSD study of the effect of electropulsing treatment on the microstructure evolution in a typical cold-deformed Ni-based superalloy. *Mater. Charact.* **2019**, *158*, 109936. [CrossRef]
9. Yang, Z.; Jiang, F.; Wang, X.B.; Qu, L.; Li, Y.G.; Chai, L.; Zhang, F.C. Effect of electropulsing treatment on microstructure and mechanical properties of a deformed ZrTiAlV alloy. *Materials* **2019**, *12*, 3560. [CrossRef]
10. Zimniak, Z.; Radkiewicz, G. The electroplastic effect in the cold-drawing of copper wires for the automotive industry. *Arch. Civ. Mech. Eng.* **2008**, *8*, 173–179. [CrossRef]
11. Lijuan, Z. Stress intensity factor analysis of space crack arresting based on flow field complex potential. *J. Yanshan Univ.*. [CrossRef]
12. Ao, D.; Chu, X.; Yang, Y.; Lin, S.; Gao, J. Effect of electropulsing treatment on microstructure and mechanical behavior of Ti-6Al-4V alloy sheet under argon gas protection. *Vacuum* **2018**, *148*, 230–238. [CrossRef]
13. Yu, W.P.; Qin, R.S.; Wu, K.M. Effect of electropulsing on grain refinement of a medium carbon low alloy steel. *Adv. Mater. Res.* **2010**, *146*, 1849–1854. [CrossRef]
14. Guo, H.; Zeng, X.; Fan, J.; Zhang, H.; Zhang, Q.; Li, W.; Dong, H.; Xu, B. Effect of electropulsing treatment on static recrystallization behavior of cold-rolled magnesium alloy ZK60 with different reductions. *J. Mater. Sci. Technol.* **2019**, *35*, 1113–1120. [CrossRef]
15. Zhan, T.; Chai, F.; Zhao, J.; Yan, F.; Wang, W. A study of microstructures and mechanical properties of laser welded joint in GH3030 alloy. *J. Mech. Sci. Technol.* **2018**, *32*, 2613–2618. [CrossRef]

16. Zhang, H.; Zhang, C.; Han, B.; Qiu, J.; Li, H.; Qin, S.; Liu, J.; Wang, Y.; Zhang, P.; Pan, Y.; et al. Evolution of grain boundary character distributions in a cold-deformed Nickel-based superalloy during electropulsing treatment. *J. Mater. Res. Technol.* **2020**, *9*, 5723–5734. [CrossRef]
17. Jin, W.; Fan, J.; Zhang, H.; Yang, L.; Dong, H.B.; Xu, B. Influence of electropulsing treatment on microstructure evolution and properties of ZK60 alloy sheets. *Rare Mater. Eng.* **2016**, *45*, 2677–2682.
18. Zhou, Y.; Zhang, W.; Wang, B.; He, G.; Guo, J. Grain refinement and formation of ultrafine-grained microstructure in a low-carbon steel under electropulsing. *J. Mater. Res.* **2002**, *17*, 2105–2111. [CrossRef]
19. Zhou, Y.; Zhang, W.; Wang, B.; Guo, J. Ultrafine-grained microstructure in a Cu-Zn alloy produced by electropulsing treatment. *J. Mater. Res.* **2003**, *18*, 1991–1997. [CrossRef]
20. Qin, S.; Zhang, H.; Liu, J.; Zheng, W. Electron backscattered diffraction analysis of the effect of deformation temperature on the microstructure evolution in a typical nickel-based superalloy during hot deformation. *J. Mater. Res.* **2016**, *31*, 1348–1360. [CrossRef]
21. Samuel, E.I.; Bhowmik, A.; Qin, R. Accelerated spheroidization induced by high intensity electric pulse in a severely deformed eutectoid steel. *J. Mater. Res.* **2010**, *25*, 1020–1024. [CrossRef]
22. Fard, R.A.; Kazeminezhad, M. Effect of electropulsing on microstructure and hardness of cold-rolled low carbon steel. *J. Mater. Res. Technol.* **2019**, *8*, 3114–3125. [CrossRef]
23. Marx, V.; Reher, F.; Gottstein, G. Simulation of primary recrystallization using a modified three-dimensional cellular automaton. *Acta Mater.* **1999**, *47*, 1219–1230. [CrossRef]
24. Salandro, W.A.; Jones, J.J.; Bunget, C.; Mears, L.; Roth, J.T. *Electrically Assisted Forming*; Springer Science and Business Media: Dordrecht, The Netherlands, 2015.
25. Bergman, Y.Z.; Kaveh, M.; Wiser, N. Explanation for the deviations from Matthiessen's rule for the low-temperature electrical resistivity of the simple metals. *Phys. Rev. Lett.* **1974**, *32*, 606–609. [CrossRef]
26. Wang, Y.; Shao, W.; Zhen, L.; Yang, L.; Zhang, X. Flow behavior and microstructures of superalloy 718 during high temperature deformation. *Mater. Sci. Eng. A* **2008**, *497*, 479–486. [CrossRef]
27. Randle, V. Twinning-related grain boundary engineering. *Acta Mater.* **2004**, *52*, 4067–4081. [CrossRef]
28. Field, D.; Bradford, L.; Nowell, M.; Lillo, T. The role of annealing twins during recrystallization of Cu. *Acta Mater.* **2007**, *55*, 4233–4241. [CrossRef]
29. Wang, F.; Qian, D.; Hua, L.; Mao, H.; Xie, L. Voids healing and carbide refinement of cold rolled M50 bearing steel by electropulsing treatment. *Sci. Rep.* **2019**, *9*, 1–7. [CrossRef]